Geoscience Letters

RESEARCH LETTER

Open Access

Probabilistic seismic hazard assessment in complex fault systems: exploring the Longitudinal Valley of Taiwan

Ting-Ying Lu[1] and Chung-Han Chan[1,2*]

Abstract

This study validates several seismic models used in PSHA studies and evaluates their impact on hazard levels in the Longitudinal Valley, Taiwan, a region with high seismic activity and data quality. The Gutenberg–Richter (G-R) law, fitting well for small to moderate magnitudes, faces uncertainties at larger magnitudes due to limited data. The pure characteristic earthquake (PCE) model assesses maximum earthquake recurrence rates for each seismogenic structure, challenging due to longer recurrence intervals. The Seismic Hazard and Earthquake Rates in Fault Systems (SHERIFS) model, incorporating the G-R law and structure parameters, forecasts seismic activity for the study region and each individual seismogenic structure. The hazard maps, assessed based on two models, reveal differences, especially around the Milun Fault and southern tip of the Longitudinal Valley. The hazard curves for cities reflect varying hazard levels influenced by nearby faults. Based on the SHERIFS model, the hazard is distributed across various faults. This indicates that the SHERIFS model effectively allocates the occurrence rates for each magnitude. This underscores the importance of multiple seismic models for precise hazard assessment, which is crucial for understanding earthquake physics and future PSHA in Taiwan.

Keywords Probabilistic seismic hazard assessment, G-R law, SHERIFS, Longitudinal Valley, Taiwan

Introduction

Probabilistic seismic hazard assessment (PSHA) plays pivotal roles in mitigating the potential devastating impact of seismic events on communities and infrastructure (e.g., Pagani et al. 2020; Woessner et al. 2015). A precise PSHA requires understanding of seismic activity in the vicinity of the site of interest. Practically, many of PSHAs implemented the Gutenberg–Richter law (also known as 'G-R law', Gutenberg and Richter 1944; Ishimoto 1939c) that defines the relationship between earthquake magnitudes (M) and the number of earthquakes (N) within a specific magnitude range, expressed by the equation:

$$\log \mathrm{N} = a - b\mathrm{M}, \tag{1}$$

where N represents number of earthquakes in a given magnitude bin, M is earthquake magnitude, and *a*- and *b*-values are parameters of the G-R law estimated through regression of earthquake parameters from a catalog. The G-R law establishes the relationship between earthquake magnitudes and the number of earthquakes within a specific magnitude range that serves as a tool for analyzing earthquake activity patterns and forecasting future earthquake occurrences.

Seismic activity in a region that covers several fault systems usually follows the G-R law (Parsons et al. 2018). However, seismicity behavior along individual fault system remains controversial. One alternative hypothesis is

*Correspondence:
Chung-Han Chan
hantijun@googlemail.com
[1] Department of Earth Sciences, National Central University, Taoyuan City, Taiwan
[2] Earthquake Disaster & Risk Evaluation and Management Center, National Central University, Taoyuan City, Taiwan

the pure characteristic earthquake model (PCE, Schwartz and Coppersmith 1984), which assumes a fault system tends to produce an earthquake with a characteristic magnitude (i.e., the largest magnitude on a fault could be estimated by the physical properties and dimensions of the fault segment). Some previous studies (e.g., Chan et al. 2020) proposed a model that follows the G-R law to illustrate seismicity rates for small earthquakes, whereas a higher rate is expected at the characteristic magnitude. Besides, Chartier et al. (2017, 2019) proposed a model, namely 'the Seismic Hazard and Earthquake Rates in Fault Systems (also known as "SHERIFS")', for evaluating seismicity rates in a fault system that involves multiple fault sections or fault-to-fault ruptures. This model allows computing earthquake rates on faults based on the geometry of fault systems and background, a list of potential earthquake ruptures, and specified rules. The underlying approach used in the program is to first estimate the moment rate available for each fault and then apply a set of rules that enable the consumption of slip rates for each fault in either single or multi-fault rupture scenarios allowed in the model until their slip-rate budget is exhausted. Since this model is applicable for a fault system with several individual faults or/and fault branches, it is ideal for application to a complex fault system. Some previous studies have utilized SHERIFS to assess seismic hazards in regions prone to complex fault interactions (e.g., Cheng et al 2023). By incorporating detailed fault geometries and considering the interactions between faults, SHERIFS provides a more accurate evaluation of seismic hazards compared to traditional models (Gómez-Novell 2020).

In this study, we aim to validate the credibility of some earthquake models frequently implemented into PSHA studies and evaluate their impacts on hazard levels. For model validation, we apply the models to the Longitudinal Valley, Taiwan, a region with high seismic activity. We first introduce the G-R law based on regression of observed seismic activity. Then we implement the PCE model to evaluate recurrence rate of the maximum earthquake for each seismogenic structure based on structure parameters. Considering the *b*-value of the G-R law and parameters of the faults, we illustrate seismicity rate through SHERIFS and discuss the rupture behavior of each individual fault. The outcomes of this study would be crucial for understanding earthquake physics and be beneficial for next-generation PSHA for Taiwan.

Seismicity and fault system along the Longitudinal Valley

To validate the reliability of different seismic models, it's crucial to apply them to an area with both a comprehensive earthquake catalog and substantial seismic activity. We thus chose the Longitudinal Valley as our study area, and the rationale behind this selection is detailed below.

Taiwan is situated in the boundary between the Eurasian Plate and the Philippine Sea Plate, with a high convergence rate (Yu et al. 1997). The boundary of these two plates on the island of Taiwan has led to the formation of the present-day the Longitudinal Valley, which stretches about 150 km in a north-northeast direction. Based on geodetic measurements, the Longitudinal Valley experiences a horizontal shortening of approximately 2–3 cm per year, accounting for 25–37% of the total east–west shortening across Taiwan (Angelier et al. 2000; Yu and Kuo 2001). Such tectonic setting results in high seismic activity along this region, including the 1951 earthquake sequence with several M7-class earthquakes, and the 2018 Hualien earthquake with M_w6.2 (Fig. 1).

Besides significant seismic activity, a comprehensive earthquake catalog is vital to ensure the quality of the model. A modern seismic network, Taiwan Telemetered Seismographic Network (TTSN), was established in Taiwan since 1972. The TTSN started with six stations in 1972 and expanded to 24 stations by 1987. The

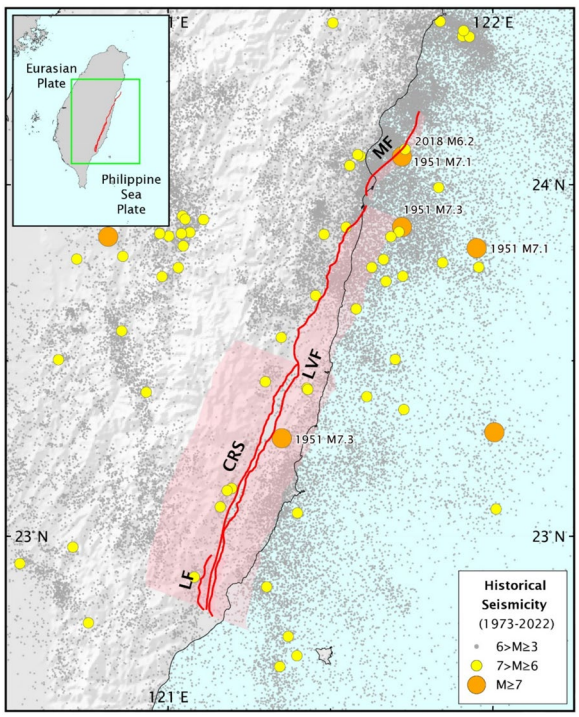

Fig. 1 The seismic activity in Eastern Taiwan. The gray dots represent earthquakes with 6 > M ≥ 3, yellow circles represent earthquakes with 7 > M ≥ 6, and orange circles represent earthquakes with M ≥ 7 from 1973 to 2022, while the beige circles represent earthquakes with M ≥ 7 from 1935 to 1972. The red alignments represent four seismogenic structures implemented in this study, including the Milun fault (MF), the Longitudinal Valley fault (LVF), the Central Range structure (CRS), and the Luyeh fault (LF). The red polygons represent the surface projection range of the faults

Table 1 The parameters of the four seismogenic structures in the study region

Seismogenic structure name	Length (km)	Depth (km)	Dip (degree)	Rake (degree)	Maximum magnitude	Slip rate (mm/year)			Recurrence interval (year)
						Min	Mean	Max	
Milun fault	32.6	10	75.0 (NE)	45	6.56	10.11	10.15	10.19	80
Longitudinal Valley fault	147.5	20	75.0 (NE)	45	7.52	5.6	11.35	17.1	200
Central Range structure	86.2	20	45.0 (NE)	90	7.38	5.51	7.28	9.05	270
Luyeh fault	19.6	4	45.0 (NE)	90	6.24	6.17	6.34	6.51	130

completeness magnitude (where all events with this magnitude or larger are well-recorded, also known as 'M_c') of the TTSN catalog is approximately 3.0 for inland regions and 4.0 for areas offshore of Taiwan (Chan 2016). Afterward, the Central Weather Bureau, former Central Weather Administration (CWA)—Taiwan's official governmental agency for broadcasting earthquake information—offers a high-quality seismographic network and provides an earthquake catalog through the Taiwan Geophysical Database Management System (GDMS, https://gdms.cwa.gov.tw). According to the study by Chan et al. (2012), M_c can be as low as 2.0 within the Taiwan Island since 1994. The Longitudinal Valley region, with its frequent and well-recorded seismic activity, provides an ideal environment for this study, enabling the effective validation of the forecasting models.

Among the seismic events in Taiwan, the 1951 Hualien-Taitung earthquake series (Fig. 1) is particularly noteworthy. It was the most destructive seismic events in the recorded history of eastern Taiwan. The sequence began on October 21, 1951, with the M_L7.3 Hualien main shock followed by a series of aftershocks greater than M_L6, including the M_L7.1 event on the Milun Fault. The subsequent M_L7.3 Yuli earthquake took place in the southern part of the Longitudinal Valley fault. Overall, the 1951 Hualien-Taitung sequence is characterized by a leaping behavior. This series involved sequential ruptures along four distinct fault segments, indicating the occurrence of multiple-fault ruptures during a single earthquake event.

The recurrence intervals of large earthquakes could also be validated using paleoseismic evidence. Chen et al. (2004) conducted a paleoseismic study on the fault associated with the 1951 Hualien earthquake. Through trench excavation and sedimentary layer analyses on the northern segment of the Longitudinal Valley fault, they identified two paleoseismic events. The most recent event was the 1951 earthquake, while the previous event occurred ca. 500–330 years before present (YBP). Based on the uplift amounts and time intervals of these two events, the recurrence interval is estimated to be less than 250 years. Besides, Tseng (2019) provided additional paleoseismic evidence for the Milun Fault, revealing significant variability in recurrence intervals. Specifically, the interval between the 1951 and 2018 events was only a few decades, whereas the intervals between earlier events, such as from 790–144 YBP to 3980–2306 YBP, spanned thousands of years.

In addition to seismic activity along the Longitudinal Valley, several seismogenic structures have been identified. Based on the seismogenic structure databased archived by the Taiwan Earthquake Model (also known as 'TEM'), there are four structures identified in the study region, those are the Milun fault, the Longitudinal Valley fault, the Central Range structure, and the Luyeh fault (Shyu et al. 2016; 2020, the structure alignments shown in Fig. 1). Based on geomorphological, geological, paleaoseismic evidence and historical events, structure parameters of these seismogenic structures have been determined (Table 1). Through the structure parameters, we evaluated seismicity rates along each structure considering different models.

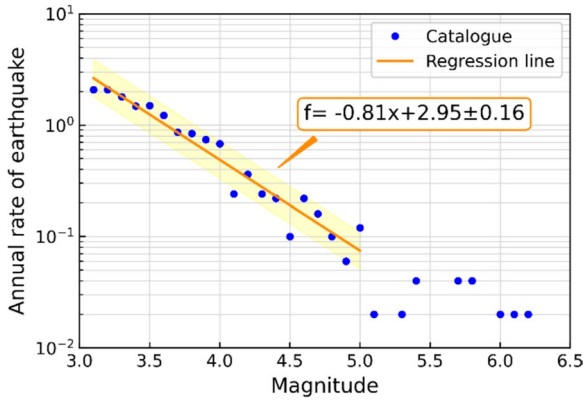

Fig. 2 The G-R law for the total of the four seismogenic structures (Milun fault, Longitudinal Valley fault, Central Range structure and Luyeh fault). The gray dots represent observations within 1 km of four seismogenic structures in the Longitudinal Valley within the red polygon in Fig. 1. The red line depicts the regression line calculated from these observational values, while the red zone represents plus or minus one standard deviation from the regression line. The observational values were obtained from TTSN data for the period 1973–1991 and GDMS data for the period 1992–2022

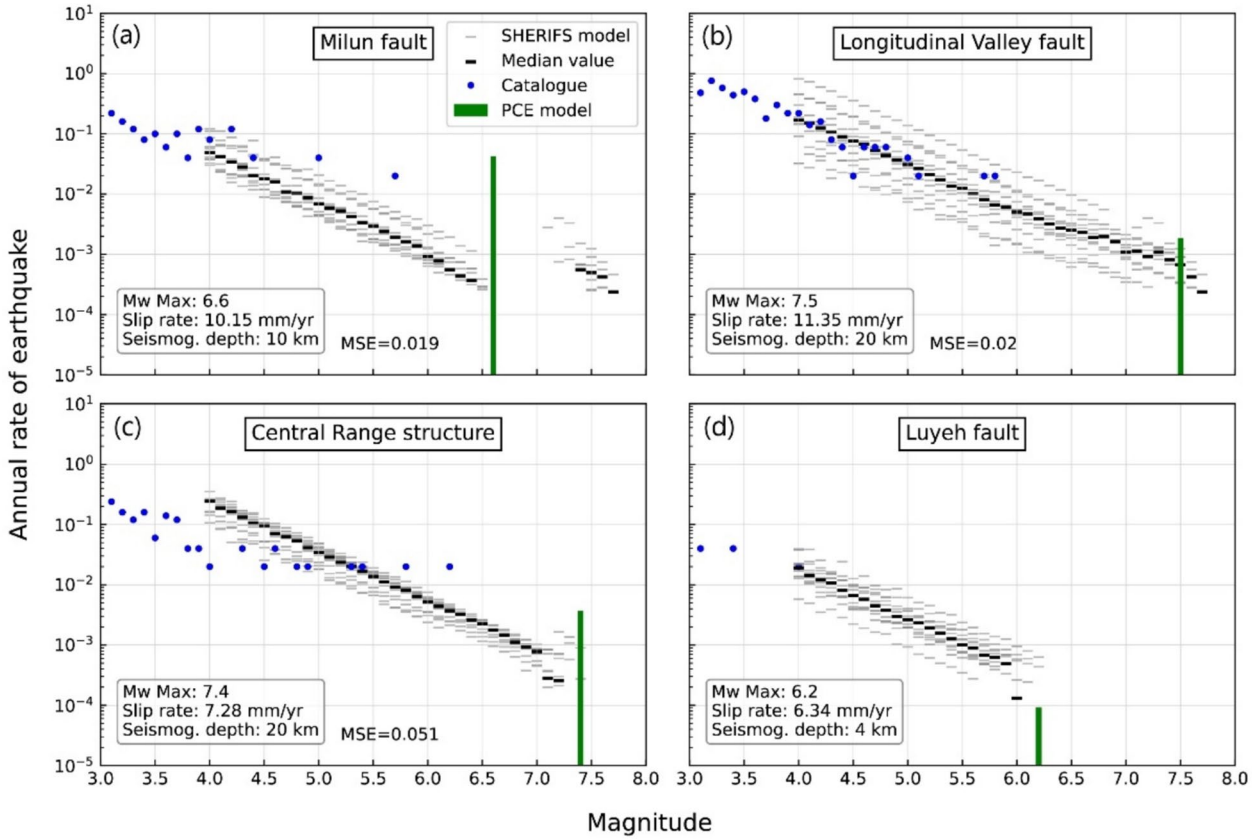

Fig. 3 A comparison between the calculated annual rates from the SHERIFS model, the PCE model and the observational data within a 1-km range from each seismogenic structure: **a** Milun fault, **b** Longitudinal Valley fault, **c** Central Range structure, and **d** Luyeh fault. Considering magnitude of completeness (M_c), we demonstrated observations for the magnitudes larger or equal to 3.0. The gray dots represent the annual earthquake rates from observations. The blue dashes represent the modeled rates from each round of SHERIFS simulation. The blue squares correspond to the median value of the modeled earthquake rates via SHERIFS. The green bars represent the characteristic magnitude and occurrence rate calculated by the PCE model. The mean-square error (MSE) for the SHERIFS model for each structure is reported

Fault rate modeled by the G-R law

The G-R law is one of popular models for applications to PSHAs that some previous studies (e.g., the national seismic hazard maps of Japan by Fujiwara and Meyers 2014) illustrated rates for areas with similar tectonic setting, and others (e.g., the national seismic hazard maps of Indonesia by Irsyam et al. 2020) evaluated seismicity rate on each fault.

We applied the G-R law to analyze earthquake activity in the Longitudinal Valley region and estimated earthquake rate with expected magnitudes as:

$$\log \mathrm{N} = 2.84 - 0.81\mathrm{M} \pm 0.19. \quad (2)$$

It shows good fit with observations (Fig. 2). In addition to the fit with seismic activity in the past, the forecasting ability of the G-R law has also been confirmed by previous studies (e.g., Chan et al. 2017). However, when this model is applied to a case with insufficient number of events, such as the part of large magnitude, the uncertainty could be raised. For example, in Fig. 2, as the magnitude increases ($M > 5.0$), the data tend to become more scattered. Such observations are fit with some previous studies (e.g., Parsons et al., 2018) that disagreed with this model for large magnitudes especially in an individual fault system. Thus, alternative models are desired to quantify seismicity rate for large magnitude.

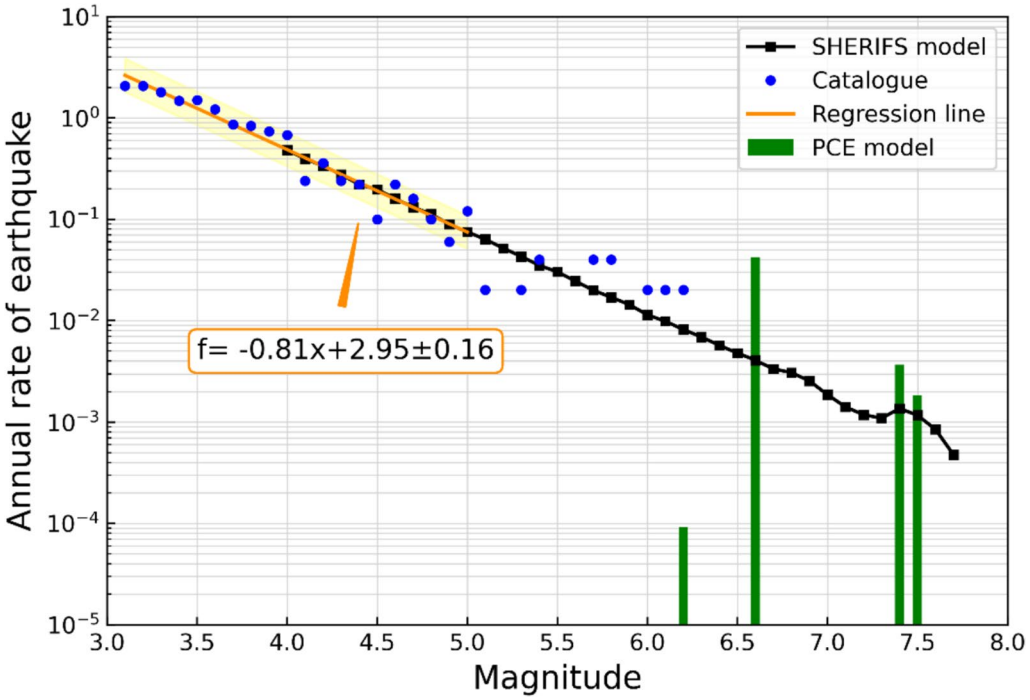

Fig. 4 A comparison between the total of modeled rates for four seismogenic structures (Milun fault, Longitudinal Valley fault, Central Range structure and Luyeh fault) from the median values of SHERIFS model and the total observational data within a 1-km range from four seismogenic structures. The red line is a regression line for observational data based on the G-R Law (represented in Fig. 2 and Eq. 2). The green bars represent the characteristic magnitudes and occurrence rates calculated by the PCE model

Fault rate modeled by the pure characteristic earthquake (PCE) model

In order to model the seismicity rate on each seismogenic structure for PSHA, the TEM implemented the PCE model that assumes the slip potency will only contribute to events with characteristic magnitude (Wang et al. 2016; Chan et al. 2020). Based on this assumption, the recurrence rate of rupture on each seismogenic structure was evaluated (Table 1). Since this model assumes seismogenic structures only rupture entirely, occurrence of smaller events could be attributed to background seismicity in the forms of area source. Combing the seismic activity from seismogenic structures through the PCE model (a peak seismicity rate is assumed for the characteristic magnitude) and background seismicity through the G-R law (i.e., the frequency–magnitude relation follows a power law for smaller magnitudes) fits the concept of the characteristic earthquake model of Schwartz and Coppersmith (1984). Since the recurrence intervals of most structures are longer than instrumental observation period (Table 1), validating the credibility of the PCE model is rather difficult. Here, we infer an anomalously short rupture cycle of only 67 years for the Milun Fault, based on the interval between the 2018 and 1951 Hualien earthquakes. This recurrence interval is close to the estimate from our PCE model, which aligns with the TEM model reported by Chan et al. (2020) and Shyu et al. (2020).

Fault rate modeled by the SHERIFS

To model seismicity based on SHERIFS, this study utilized structure geometries, and slip rates of the four seismogenic structures (Table 1). This study considered a shape of Magnitude-Frequency Distribution (MFD) that fits the G-R law. In order to make the MFD more representative of real conditions, this study considers the *b*-value of 0.81 from Eq. (2) to control the slope of the MFD. We assumed that all of the slip potency contributes to seismicity on each seismogenic structures, rather than background activity. Since SHERIFS allows an earthquake that rupture on multiple faults, this study followed the conclusion of Shyu et al. (2020) and assumed that the Milun fault and the Longitudinal Valley fault may rupture simultaneously in a coseismic period.

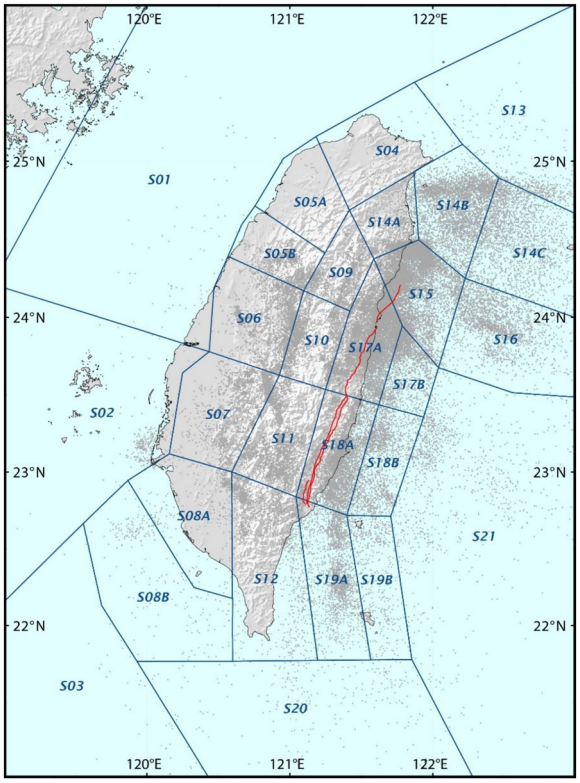

Fig. 5 The distribution of the 28 area sources and seismicity based on the catalog over 50 years

Modeled seismicity rate on each fault/structure is shown in Fig. 3. Since SHERIFS assumes possibilities of multi-fault ruptures, a larger event is expected than the characteristic magnitude. For example, the characteristic magnitude of the Milun fault is 6.56 (Table 1), an earthquake with magnitudes ranging from M7.5 to M7.7 is expected during a multiple-fault rupture with the Longitudinal Valley fault. Such assumption fit the occurrence of the 1951 sequence that initiated with the M_L 7.3 on the Longitudinal Valley fault, followed by a M_L 7.1 at North on the Milun fault (Chen et al. 2008). The jumping rupture phenomenon of the 1951 sequence was previously confirmed by Chen et al. (2008), who used a combination of static stress transfer and rate/state stress transfer models to explain the rupture behavior along four distinct fault segments. Their modeling results highlighted the importance of the physical properties associated with the high seismicity of the Chihshang segment in understanding the triggering of the jumping rupture. Additionally, they investigated the temporal variation in fault segmentation by measuring rate/state friction parameters across various segments of the Longitudinal Valley fault. Our SHERIFS model suggests shorter recurrence intervals for single-fault ruptures and longer intervals for multi-fault ruptures (Fig. 3a). This phenomenon is consistent with the paleoseismic data (Tseng 2019) mentioned in Chapter 2, thus providing preliminary validation for the performance of the SHERIFS model on the Milun fault. It is important to note that certain events might be missing from the excavation site. If this is the case, it could indicate shorter recurrence intervals, aligning more closely with the PCE model (Fig. 3a).

In order to validate the performance of the SHERIFS model, this study compared the models with observations. The observational data utilized in this study are derived from the seismic catalogs of TTSN and GDMS. The TTSN operated from 1973 to 1991 while the GDMS data archived earthquake catalog from 1992 to 2022, encompassing a total observation period of 50 years. The spatial distribution of earthquakes is depicted in Fig. 1. We presented observed MFD for the seismicity within 1 km from each seismogenic structure, shown as gray dots in Fig. 3. Based on reported mean-square error (MSE), SHERIFS excellently represents the occurrence rates of earthquakes of various magnitudes and appropriately allocates the budget provided by slip rate to each magnitude. Furthermore, it successfully presents the probability of multiple-fault ruptures, fit the experience of the 1951 earthquake sequence (Fig. 1).

In addition to model the seismicity rate for each seismogenic structure, we further applied the SHERIFS model to the entire Longitudinal Valley region, a fault system that consists of four seismogenic structures (Fig. 4). Comparing the seismicity within each seismogenic structure and the modeled rate from the entire Longitudinal Valley region, the SHERIFS model (i.e., shown in blue line) performed well in forecasting MFD (shown in Fig. 4).

A traditional G-R law model exhibits limitations in accurately forecasting large magnitude earthquakes due to significant deviations in earthquake frequency (Fig. 2). Consequently, an extended recording period is preferable for determining a consistent seismicity rate. In contrast, SHERIFS showcases its proficiency in forecasting seismic activities of larger magnitudes, inclusive of earthquakes induced by multi-fault ruptures, i.e., modeled rate for the Milun and the Longitudinal Valley faults (Fig. 3). This highlights the advanced capability of the SHERIFS model, especially pertinent for evaluating seismic hazards in

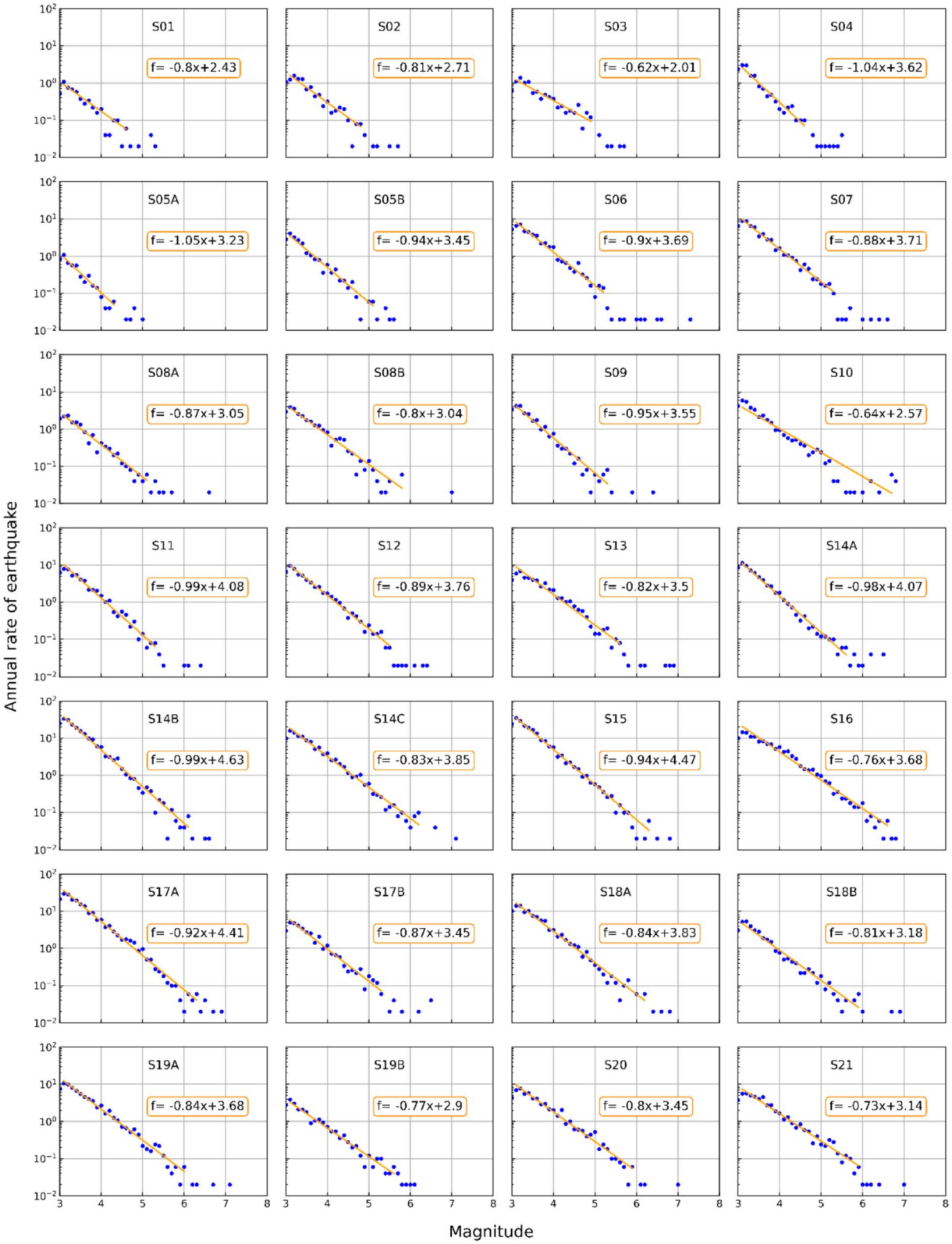

Fig. 6 The calculated *a*- and *b*-values for the 28 area sources based on the catalog over 50 years. The distribution of the 28 area sources is depicted in Fig. 5

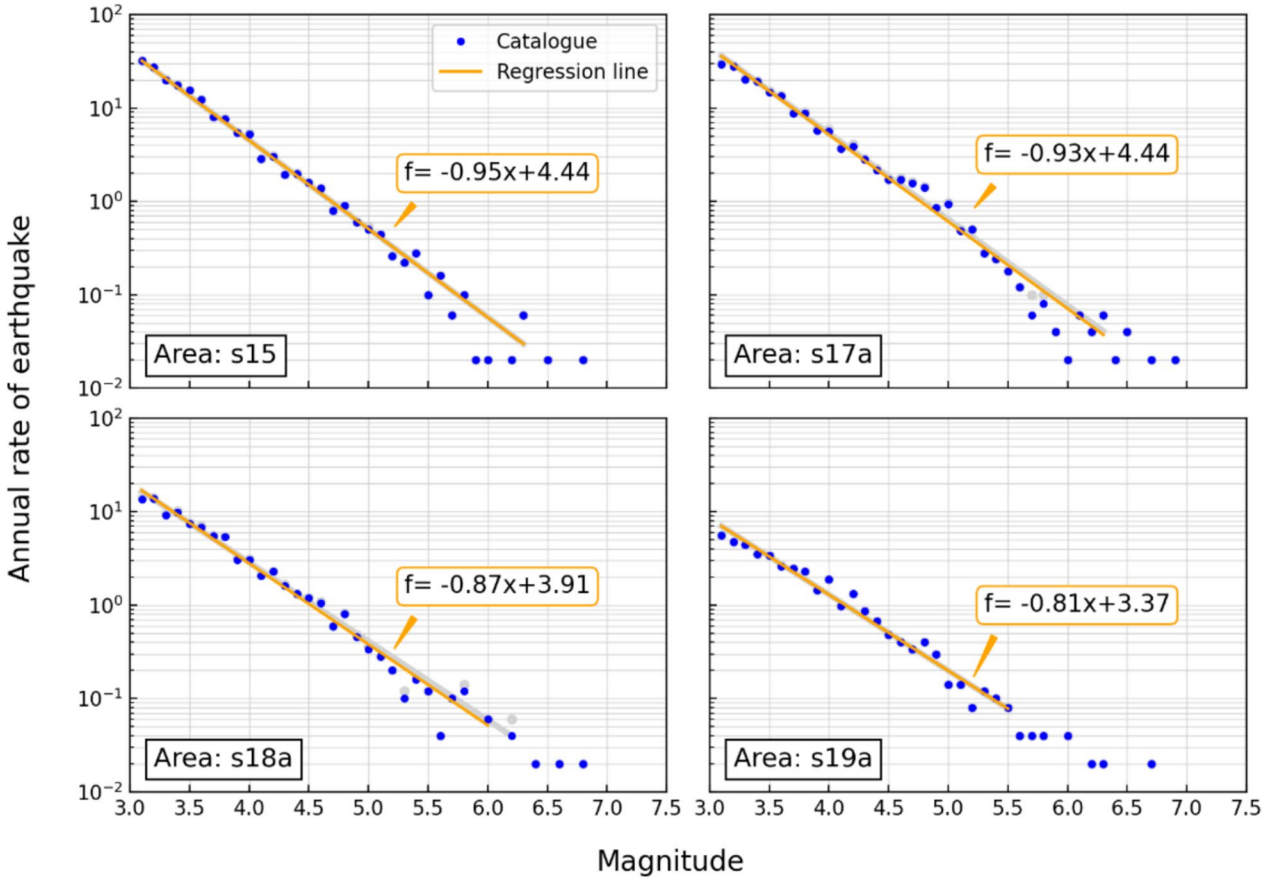

Fig. 7 The modified parameters of three area sources of SHERIFS model. The gray dots and red lines represent the old calculated parameters used for the PCE model, which are identical to those in Fig. 6, while the modified parameters are shown as black dots and black lines

areas with complex fault system. Noteworthily, SHERIFS aligns with the characteristic earthquake model (Youngs and Coppersmith 1985), factoring in scenarios with multi-fault ruptures. This suggests that the SHERIFS model may offer a more comprehensive understanding of the complexities of seismic events and the relationships among various faults, providing a precise model for subsequent probabilistic seismic hazard assessments (Fig. 5).

Probabilistic seismic hazard assessment for the Longitudinal Valley

In order to quantify the impact various earthquake models on hazard level, this study utilized PSHA through the open-source software OpenQuake engine (Pagani et al. 2014). The GMPEs utilized in this study is proposed by Lin et al. (2011), while the V_s^{30} values considered for site effects are sourced from Taiwan Strong Motion Instrumentation Program network (TSMIP) stations provided by Engineering Geological Database for TSMIP (EGDT, https://egdt.ncree.org.tw). Based on the polygons of the area sources are derived from Chan et al. (2020), the *a*- and *b*-values for each area were determined using seismic data spanning 50 years (Fig. 6). Meanwhile, the area sources corresponding to the SHERIFS model were modified from the former, with adjustments tailored to the Longitudinal Valley region. Specifically, seismicity within 1 km of each fault were excluded, and new *a*- and *b*-values were determined to represent the updated area sources (Fig. 7). As for seismogenic structures and fault sources, the parameters used for the PCE model are shown as the green bars in Fig. 3, considering their respective maximum probable earthquakes and occurrence rates. Meanwhile, the SHERIFS model considers the median of MFD in Fig. 3, as well as the possibility of multiple-fault ruptures.

Based on the models mentioned above, we assessed probabilistic seismic hazards and presented the results in the forms of hazard maps (Fig. 8) and hazard curves

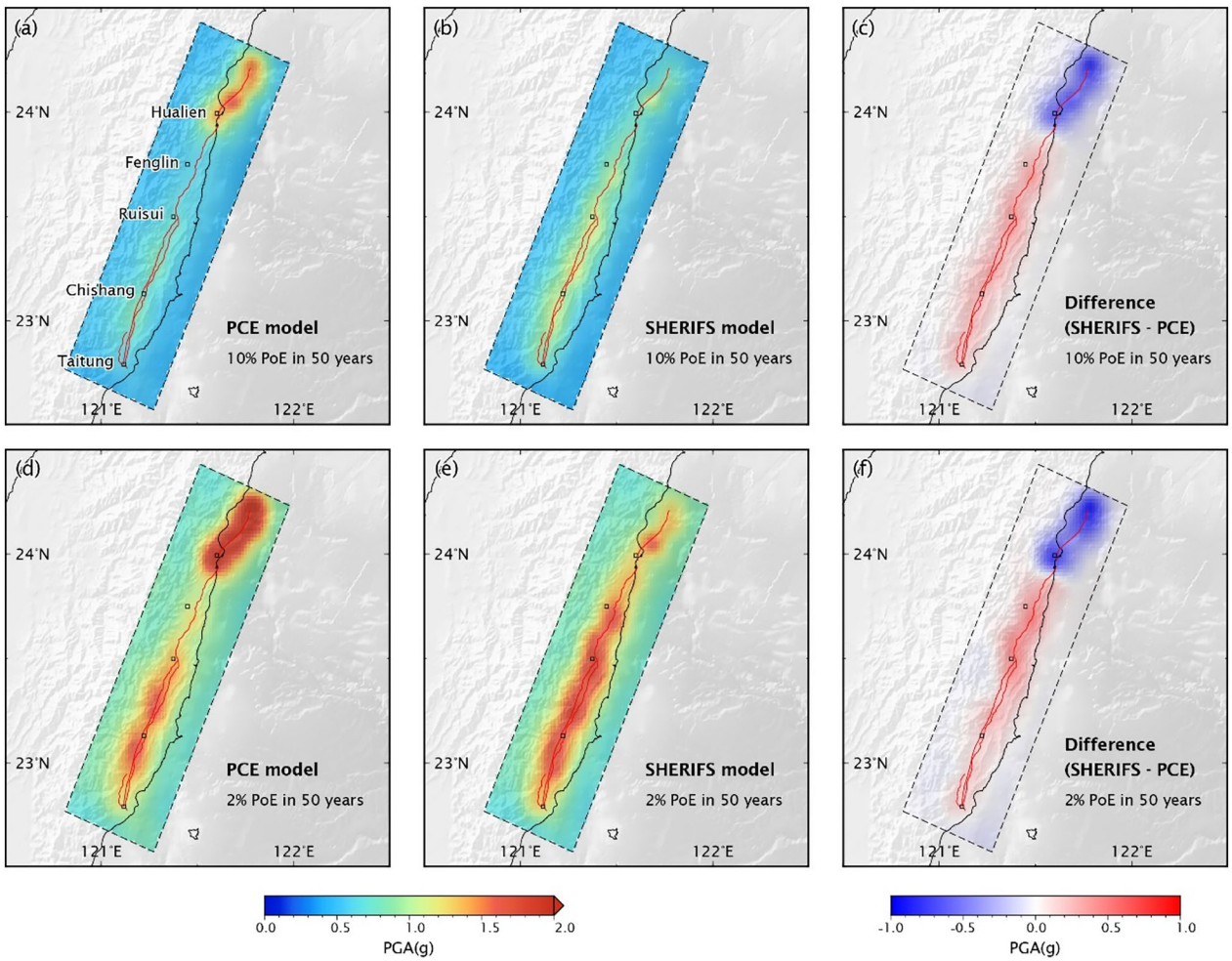

Fig. 8 **A** The hazard maps for PGA (g) of the PCE for 10% PoE in 50 years; and **B** the SHERIFS model for 10% PoE in 50 years; **C** difference (in g) of the hazard maps from the PCE model respective to the SHERIFS model for 10% PoE in 50 years; **D** the hazard maps for PGA (g) of the PCE model for 2% PoE in 50 years; and **E** the SHERIFS model for 2% PoE in 50 years; **F** difference (in g) of the hazard maps from the PCE model respective to the SHERIFS model for 2% PoE in 50 years. The color scale is identical for both PoEs. The traces of the four seismogenic structures are depicted in red in all panels

for five cities in the region (Fig. 9). In the comparison of the two models at a 10% Probability of Exceedance (PoE) in 50 years (corresponding to a 475-year return period), the hazard based on the PCE model is slightly high around the Milun Fault (Fig. 8a), while based on the SHERIFS model, the hazard is distributed across various faults (Fig. 8b). Such results could be attributed to higher rates of activity along the Milun fault in the PCE model (Fig. 3a) and to other seismogenic structures in the SHERIFS model (Fig. 3b–d). Furthermore, at a 2% PoE in 50 years (equivalent to a 2475-year return period), this phenomenon is even more pronounced (Fig. 8d and e). Additionally, we presented hazard curves based on different models for the five cities from Hualien to Taitung (Fig. 9). The SHERIFS model indicates a higher hazard level for a high probability of exceedance (PoE), whereas the PCE model predicts a higher hazard for a lower PoE.

In order to confirm the hazard source for each city, we examined hazard curve for each individual seismogenic source, as illustrated in Fig. 10. The hazard in Hualien is primarily derived from the Milun Fault, which perfectly illustrates the feature of the model (Fig. 3a). In both models, all other cities are primarily influenced by neighboring faults, with the exception of the Luyeh fault. The

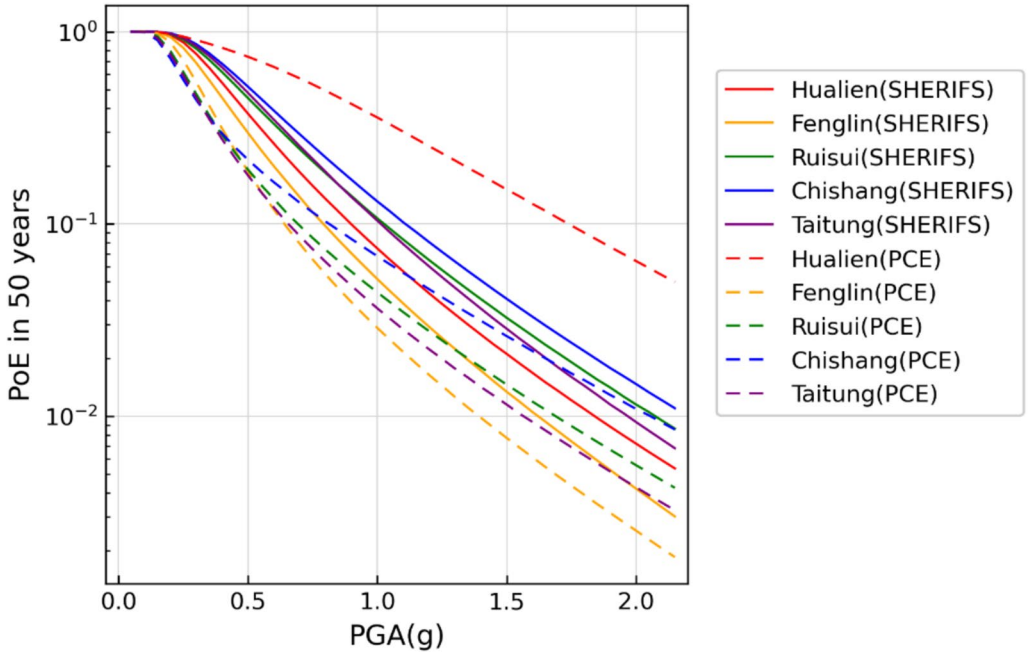

Fig. 9 The hazard curves for PGA (g) based on the PCE and SHERIFS models for the cities of Hualien, Fenglin, Ruisui, Chishang and Taitung. Their locations are indicated in the maps from Fig. 8A

Luyeh fault, which has a low slip rate and is not very long, is unlikely to generate very large-magnitude earthquakes with a short recurrence interval (Fig. 3d). The decomposed hazard curves (Fig. 10) show that area sources (earthquakes that cannot be associated with any specific seismogenic structure) contributed significant hazard for small to moderate ground shaking, whereas the fault source dominant the hazard for large ground shaking.

Conclusions

We conducted a comprehensive evaluation of probabilistic seismic hazard assessment (PSHA) in the Longitudinal Valley of Taiwan, a region characterized by high seismic activity and a complex fault system. Our investigation focused on three seismic models: the Gutenberg–Richter (G-R) law, the pure characteristic earthquake (PCE) model, and the Seismic Hazard and Earthquake Rates In Fault Systems (SHERIFS) model.

Firstly, we applied the G-R law, which demonstrated a good fit with observational seismic activity for smaller to moderate magnitudes. However, for larger magnitudes, especially within individual fault systems, the uncertainty increased due to insufficient data, highlighting the limitations of this model. Secondly, we implemented the PCE model, which assumes that each seismogenic structure produces earthquakes of characteristic magnitudes. While this model provided valuable insights into recurrence rates, validating its credibility proved challenging due to the long recurrence intervals of most structures compared to the observation period. Finally, we utilized the SHERIFS model, which accounts for multiple-fault ruptures in complex fault systems. By considering the geometry and slip rates of the seismogenic structures, SHERIFS successfully forecasted regional seismicity and aligned well with historical records, including the occurrence of multi-fault rupture events.

Our findings highlight the importance of utilizing sophisticated models like SHERIFS in PSHAs, particularly for regions with complex fault systems. Additionally, the PCE model provides valuable insights into paleoseismic activity and the short rupture cycle of the Milun Fault. By integrating various seismic models, we conducted PSHAs for the Longitudinal Valley, revealing significant variations in hazard levels across different seismogenic structure sources. We also suggest using a logic tree framework to integrate both models,

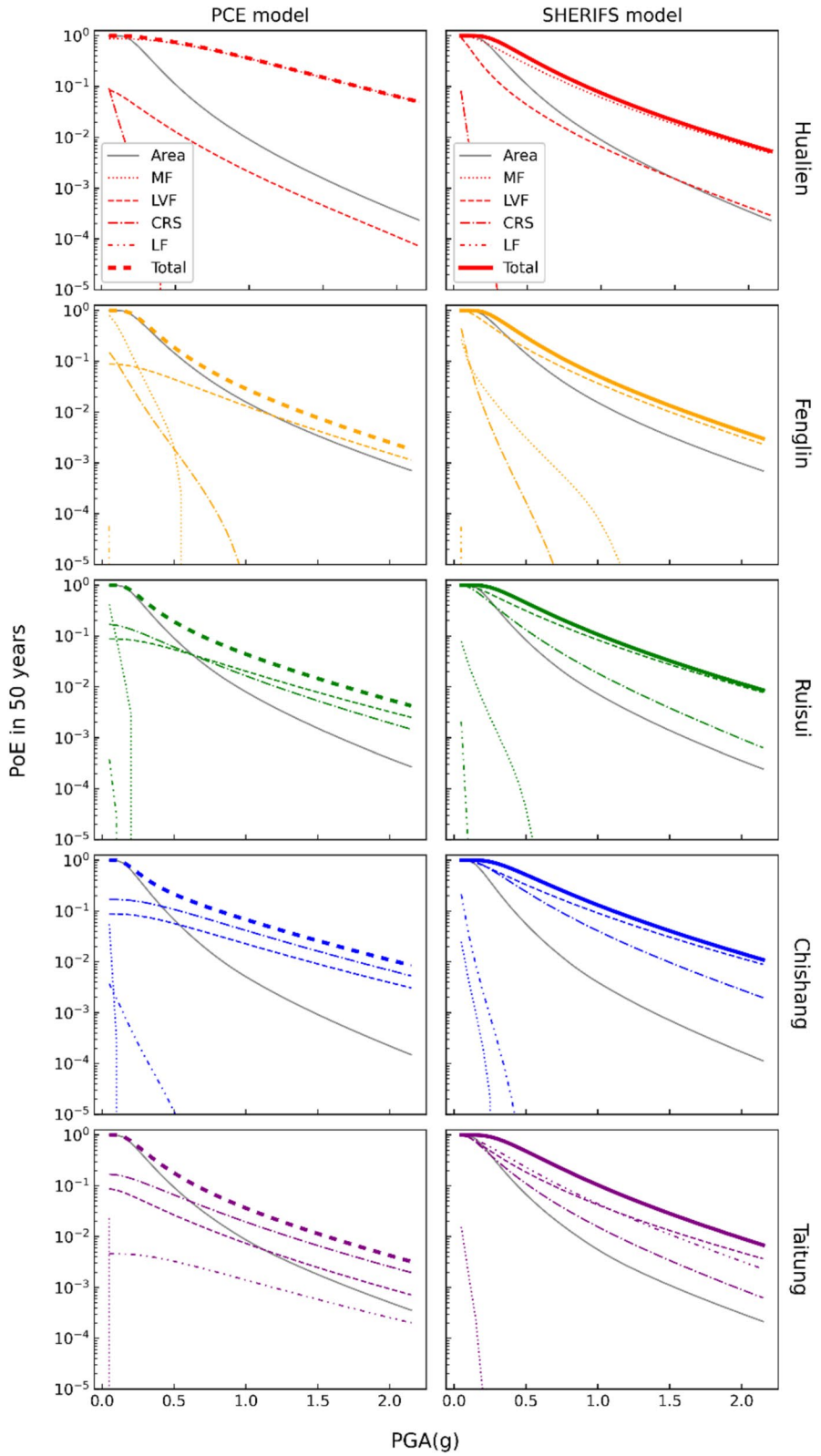

Fig. 10 The decomposed hazard curves for PGA (g) of the PCE and SHERIFS models in five cities. The different lines represent the hazards from various structures: the Milun fault (MF), Longitudinal Valley fault (LVF), Central Range structure (CRS), and Luyeh fault (LF)

effectively addressing epistemic uncertainty. This study contributes to a better understanding of earthquake physics and provides valuable insights for next-generation PSHA efforts in Taiwan. The outcomes presented here can inform seismic risk mitigation strategies and help enhance community resilience to seismic events in the Longitudinal Valley and similar tectonically active regions worldwide.

Author contributions

Both authors collaboratively developed the conception and design of the work. TL primarily performed the analyses and drafted the manuscript. CH provided supervision, offering guidance in data analysis and interpretation. Both authors actively discussed the results and significantly contributed to the manuscript's writing and revision.

Funding

This study was supported by the National Science and Technology Council in Taiwan—under grants MOST 109-2116-M-008-029-MY3, MOST 110-2124-M-002-008, and MOST 110-2634-F-008-008. This work is financially supported by the Earthquake Disaster & Risk Evaluation and Management Center (E-DREaM) from the Featured Areas Research Center Program within the framework of the Higher Education Sprout Project by the Ministry of Education in Taiwan.

Availability of data and materials

The earthquake catalog used in this study is available from the Taiwan Geophysical Database Management System (GDMS) at https://gdms.cwa.gov.tw.

Declarations

Competing interests

The authors declare no competing interests.

Received: 11 June 2024 Accepted: 22 March 2025
Published online: 09 April 2025

References

Angelier J, Chu HT, Lee JC, Hu JC (2000) Active faulting and earthquake hazard: the case study of the Chihshang fault. Taiwan. J Geodyn 29(3–5):151–185

Chan CH (2016) Importance of three-dimensional grids and time-dependent factors for applications of earthquake forecasting models to subduction environments. Nat Hazard 16(9):2177–2187

Chan CH, Wu YM, Tseng TL, Lin TL, Chen CC (2012) Spatial and temporal evolution of b-values before large earthquakes in Taiwan. Tectonophysics 532:215–222

Chan CH, Wang Y, Wang YJ, Lee YT (2017) Seismic-hazard assessment over time: Modeling earthquakes in Taiwan. Bull Seismol Soc Am 107(5):2342–2352

Chan CH, Ma KF, Shyu JBH, Lee YT, Wang YJ, Gao JC, Rau RJ (2020) Probabilistic seismic hazard assessment for Taiwan: TEM PSHA2020. Earthq Spectra 36(1_suppl):137–159

Chartier T, Scotti O, Lyon-Caen H, Boiselet A (2017) Methodology for earthquake rupture rate estimates of fault networks: example for the western Corinth rift, Greece. Nat Hazard 17(10):1857–1869

Chartier T, Scotti O, Lyon-Caen H (2019) SHERIFS: open-source code for computing earthquake rates in fault systems and constructing hazard models. Seismol Res Lett 90(4):1678–1688

Chen WS, Yen YC, Yang CC, Yang HC, Chen YQ, Tsai KZ, Huang NW, Chu YG, Chang HC, Lin CW, Lin WH, Liou Y-Q (2004) Paleoseismologic studies of the 1951 earthquake rupture, Eastern Taiwan. Central Geol Survey Spec Publ 15:137–145

Chen KH, Toda S, Rau RJ (2008) A leaping, triggered sequence along a segmented fault: the 1951 ML 7.3 Hualien-Taitung earthquake sequence in eastern Taiwan. J Geophys Res Solid Earth. https://doi.org/10.1029/2007JB005048

Cheng J, Xu C, Ma J, Xu X, Zhu P (2023) From active fault segmentation to risks of earthquake hazards and property and life losses—a case study from the Xianshuihe-Xiaojiang fault zone. Sci China Earth Sci 66(6):1345–1364

Fujiwara H, Meyers RA (2014) Seismic hazard maps for Japan. In: Encyclopedia of complexity and systems science, pp 1–28

Gómez-Novell O, García-Mayordomo J, Ortuño M, Masana E, Chartier T (2020) Fault system-based probabilistic seismic hazard assessment of a moderate seismicity region: The eastern Betics shear zone (SE Spain). Front Earth Sci 8:579398

Gutenberg B, Richter CF (1944) Frequency of earthquakes in California. Bull Seismol Soc Am 34(4):185–188

Irsyam M, Cummins PR, Asrurifak M, Faizal L, Natawidjaja DH, Widiyantoro S et al (2020) Development of the 2017 national seismic hazard maps of Indonesia. Earthq Spectra 36(1_suppl):112–136

Ishimoto M (1939) Observation of earthquakes registered with the microseismograph constructed recently (I). Bull Earthq Res Inst Univ Tokyo 17:443

Pagani M, Monelli D, Weatherill G, Danciu L, Crowley H, Silva V, Vigano D (2014) OpenQuake engine: an open hazard (and risk) software for the global earthquake model. Seismol Res Lett 85(3):692–702

Pagani M, Garcia-Pelaez J, Gee R, Johnson K, Poggi V, Silva V et al (2020) The 2018 version of the global earthquake model: hazard component. Earthq Spectra 36(1_suppl):226–251

Schwartz DP, Coppersmith KJ (1984) Fault behavior and characteristic earthquakes: examples from the Wasatch and San Andreas fault zones. J Geophys Res Solid Earth 89(B7):5681–5698

Shyu JBH, Yin YH, Chen CH, Chuang YR, Liu SC (2020) Updates to the on-land seismogenic structure source database by the Taiwan Earthquake Model (TEM) project for seismic hazard analysis of Taiwan. Terr Atmos Ocean Sci. https://doi.org/10.3319/TAO.2020.06.08.01

Tseng YC (2019) Paleoseismic study of Milun active fault in Hualien, Eastern Taiwan (Master's thesis). Graduate Institute of Applied Geology, National Central University, Taiwan

Wang YJ, Chan CH, Lee YT, Ma KF, Shyu JBH, Rau RJ, Cheng CT (2016) Probabilistic seismic hazard assessment for Taiwan. Terr Atmos Ocean Sci 27(3):325–340

Woessner J, Laurentiu D, Giardini D, Crowley H, Cotton F, Grünthal G et al (2015) The 2013 European seismic hazard model: key components and results. Bull Earthq Eng 13:3553–3596

Youngs RR, Coppersmith KJ (1985) Implications of fault slip rates and earthquake recurrence models to probabilistic seismic hazard estimates. Bull Seismol Soc Am 75(4):939–964

Yu SB, Kuo LC (2001) Present-day crustal motion along the Longitudinal Valley Fault, eastern Taiwan. Tectonophysics 333(1–2):199–217

Yu SB, Chen HY, Kuo LC (1997) Velocity field of GPS stations in the Taiwan area. Tectonophysics 274(1–3):41–59

Publisher's Note